Large-Signal Modeling of Self-Heating, Collector Transit-Time, and RF-Breakdown Effects in Power HBT's

Ce-Jun Wei, *Member, IEEE*, James C. M. Hwang, *Fellow, IEEE*, Wu-Jing Ho, *Member, IEEE*, and J. Aiden Higgins, *Senior Member, IEEE*

Abstract— **A large-signal heterojunction bipolar transistor (HBT) model has been developed which includes self-heating, collector transit-time, and RF-breakdown effects. The model has a compact form which is based on a compromise between accuracy and utility. As such, the model can be readily extracted and verified with the aid of RF waveform measurements. Using the model in simulations, it was found that RF breakdown was dependent on base biasing and loading conditions. Therefore, with proper circuit design, the maximum output power of the HBT can significantly exceed the limit of open-base breakdown voltage.**

I. Introduction

CONVENTIONAL Ebers–Moll and Gummel-Poon models are not suitable for microwave power heterojunction bipolar transistors (HBT's) because they do not include several important effects such as self heating, collector transit-time, and breakdown [1]. To date, many HBT models have included the self-heating effect [2]–[8]. A few HBT models have also included the collector transit-time effect [9]–[11]. In comparison, reports on HBT breakdown are limited to device physics and power performance [12], [13], but not the incorporation of breakdown in a compact model for circuit simulation. This is because the HBT tends to burn out under dc breakdown characterization and the correlation between dc and RF breakdown characteristics are not straight forward. On separate occasions, we have treated the self-heating [14], [15], collector transit-time [16], [17], and RF-breakdown effects [18]. Recently, for the first time, we modeled all three effects together [19]. This paper expands on [19] mainly by using the model in power performance simulation and by discussing the effect of breakdown on power performance. In the future, the breakdown effect can become even more critical as improvements are made to reduce the HBT thermal resistance and nonuniformity, so that breakdown becomes the limiting factor for HBT power performance and reliability [20].

The present model has a compact form which is based on a compromise between accuracy and utility. As such, the model can be readily extracted and verified with the aid of RF waveform measurements. The model has been implemented in a commercially available harmonic-balance circuit simulator in terms of user-defined elements. This allows the breakdown effect on HBT power performance to be conveniently evaluated as illustrated below.

Manuscript received April 1, 1996.

C.-J. Wei and J. C. M. Hwang are with Lehigh University, Bethlehem, PA 18015 USA.

W.-J. Ho and J. A. Higgins are with Rockwell International, Thousand Oaks, CA 91360 USA.

Publisher Item Identifier S 0018-9480(96)08564-X.

II. Model Construction

The present large-signal model is based on an equivalent circuit (Fig. 1) similar to that of a small-signal model [21]. This facilitates the separation of linear and nonlinear model elements. The linear elements include the intrinsic base resistance (R_{B2}), three terminal resistances (R_B, R_E, and R_C), and three terminal inductances (L_B, L_E, and L_C). The nonlinear elements include five diodes: D_F and D_E represent the injection and recombination currents, respectively, through the base-emitter junction; D_R and D_C represent similar currents through the base-collector junction; D_X represents the leakage current though the extrinsic base-collector junction. The I-V characteristics across each diode can be expressed in the following form by adding the appropriate subscript F, E, R, C, or X:

$$I_D = I_S\{\exp(V/nV_T) - 1\} \tag{1}$$

where I_S is the saturation current, n is the ideality factor, and V_T is the thermal voltage. The diode currents I_{DF} and I_{DR}, in turn, introduce current sources I_F and I_R at the base-collector and base-emitter junctions, respectively. These current sources can be expressed in the following form by adding the appropriate subscript F or R:

$$I = \alpha I_D \tag{2}$$

where α is the current gain factor. Additional nonlinear elements to account for the self-heating, collector transit-time, and breakdown effects are discussed next.

A. Self-Heating Model

The self-heating effect is manifested mainly in the reduction of junction turn-on voltage and collector current. To model such an effect, temperature-dependent voltage and current sources having the following forms are added to the base and collector, respectively, as in the following:

$$\Delta V_B = -a\Delta T \tag{3}$$

$$\Delta I_C = I_C\{1 - \exp(-b\Delta T)\} \tag{4}$$

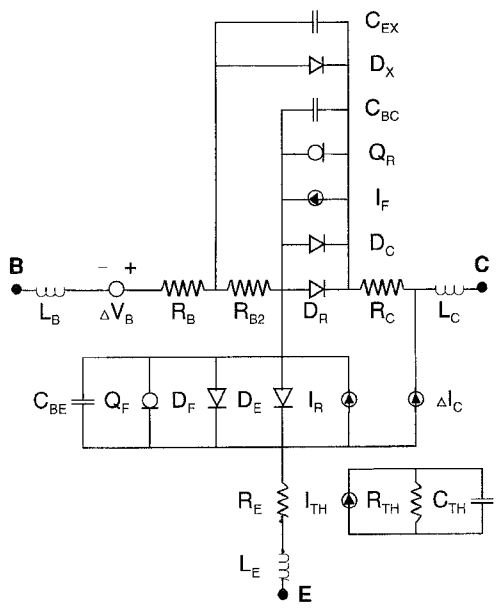

Fig. 1. Large-signal HBT equivalent circuit model.

where a and b are fitting parameters; ΔT is the normalized junction temperature rise for unity thermal resistance. Notice that the location of ΔV_B allows it to affect the turn-on voltage of both the base-emitter and base-collector junctions. To model the interaction between electrical and thermal effects, a thermal equivalent circuit was added to the electrical equivalent circuit as shown in Fig. 1. The thermal equivalent circuit consists of a unity thermal resistance $R_{TH} = 1$, a thermal capacitance C_{TH} which is the same as the temperature rise time τ_{TH} when $R_{TH} = 1$, and a thermal current I_{TH} which is proportional to the power dissipated on the HBT. As will be described in Section III, a and b can be extracted directly from I-V characteristics without knowing R_{TH}. Therefore, by using a unity thermal resistance and a normalized temperature rise, three instead of four parameters are required to model the self-heating effect. Once the thermal equivalent circuit is constructed, the instantaneous electrical current and voltage, I_C and V_{CE}, are used to evaluate the power dissipation $I_{TH} \cdot I_{TH}$ causes a temperature rise of ΔT which is in turn used to evaluate ΔV_B and ΔI_C according to (3) and (4), respectively.

B. Collector Transit-Time Model

Conventional Ebers-Moll and Gummel-Poon models use only the base-emitter charge $Q_F = I_{DF}\tau_F$ with one time constant τ_F to account for the transit-time effect under forward operation. This is, however, not accurate for power HBT's in which the collector transit time τ_C can be much longer than the base transit or diffusion time [18]. To include the collector transit-time effect, we add to the base-collector charge Q_R a second term which is proportional to τ_C and critical under forward operation also

$$Q_R = I_{DR}\tau_R + I_{DF}\tau_C. \tag{5}$$

This in turn gives rise to a transcapacitance which is a function of V_{BE}:

$$C_{BCBE} = \partial Q_R/\partial V_{BE}. \tag{6}$$

For the sake of utility, Q_F and Q_R are kept separate from the conventional junction capacitances, C_{BE}, C_{BC}, and C_{EX}. Thus, C_{BE}, C_{BC}, and C_{EX} maintain their conventional form of an abrupt junction capacitance:

$$C = C_{J0}/(1 - V/V_{J0})^{1/2}. \tag{7}$$

Further, the intrinsic base-collector capacitance is modified so that it decreases with increasing injection current

$$C'_{BC} = C_{BC}(1 - I_F/I_0). \tag{8}$$

C. Breakdown Model

Under the gross assumption that the time dependence of the avalanche breakdown process can be absorbed in the frequency dependence of the breakdown voltage, only two multiplication factors are required to modify the injection and leakage currents between the base and collector

$$\alpha'_F = m_1\alpha_F \tag{9}$$

$$I'_{SC} = m_2 I_{SC} \tag{10}$$

where m_1 and m_2 depend on the open-base breakdown voltage BV_{CEO} and open-emitter breakdown voltage BV_{CBO} according to the following:

$$m_1 = 1/\{1 - (1 - \alpha)(V_{CB}/BV_{CEO})^{\eta}\} \tag{11}$$

$$m_2 = 1/\{1 - (V_{CB}/BV_{CBO})^{\eta}\} \tag{12}$$

where η is another fitting parameter. Were there no distinction between the injection and leakage currents, (11) and (12) would have been the same because

$$BV_{CEO} = BV_{CBO}(1 - \alpha_F)^{1/\eta}. \tag{13}$$

By distinguishing the two different breakdown mechanisms under RF conditions, we allow BV_{CBO} to deviate significantly from its dc value as has been shown in [19].

To make the model more compact, (11) and (12) can be approximated by the following:

$$m_1 = \exp\{(1/\alpha - 1)(V_{CB}/BV_{CEO})^{\eta}\} \tag{14}$$

$$m_2 = \exp\{(V_{CB}/BV_{CBO})^{\eta}\}. \tag{15}$$

The above multiplication factors are applicable to conduction currents only. From small-signal S-parameters and large-signal waveforms measured under extreme bias conditions, the effect of breakdown on displacement currents was found negligible.

In summary, seven special model parameters have been introduced in the above. They include a, b, and τ_{TH} for the self-heating effect, τ_C for the collector transit-time effect, and BV_{CEO}, BV_{CBO}, and η for the breakdown effect.

III. Model Extraction

Models have been extracted from HBT's similar to that of [18], except that the collector doping was reduced to improve breakdown. The emitter area remains approximately 360 μm^2. Under a common- emitter configuration, the cut-off frequency and the maximum frequency of oscillation were measured to be 40 and 32 GHz, respectively. The maximum output power

TABLE I
LARGE-SIGNAL MODEL PARAMETERS

Linear Electrical	Nonlinear Electrical	Heating & Breakdown
R_B = 0.45 Ω	I_{SF} = 5.4×10^{-21} A; n_F = 1.2	a = 0.47 V/W
R_E = 1.1 Ω	I_{SE} = 3.0×10^{-17} A; n_E = 1.9	b = 1.5 /W
R_C = 0.72 Ω	$I_{SR} = I_{SE}\alpha_F/\alpha_R$; n_R = 1.6	τ_{TH} = 18 μs
L_B = 0.16 nH	I_{SC} = 5.1×10^{-15} A; n_C = 2.1	BV_{CEO} = 16 V
L_E = 0	I_{SX} = 2×10^{-19} A; $n_X = n_C$	BV_{CBO} = 26 V
L_C = 0.21 nH	α_F = 0.99; α_R = 0.1	η = 6.5
R_{B2} = 2.3 Ω	τ_F = 0.1 ps; τ_R = 10 ps; τ_C = 5.3 ps	
	C_{JE0} = 0.40 pF; V_{JE0} = 1.2 V	
	C_{JC0} = 0.23 pF; I_0 = 0.95 A	
	C_{EX0} = 0.18 pF; V_{JC0} = 1.1 V	

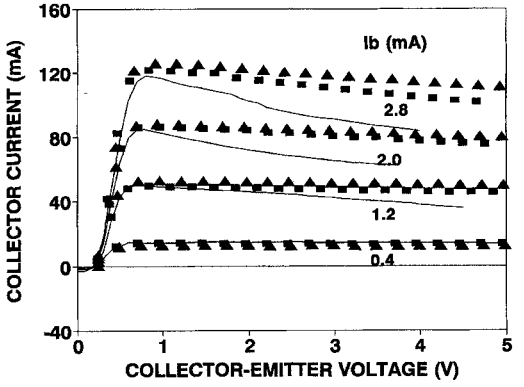

Fig. 2. Self-heating effect illustrated by collector I-V characteristics measured under (—) dc, (■) 10 μs pulse with 10% duty factor, and (▲) 1 μs pulse with 10% duty factor.

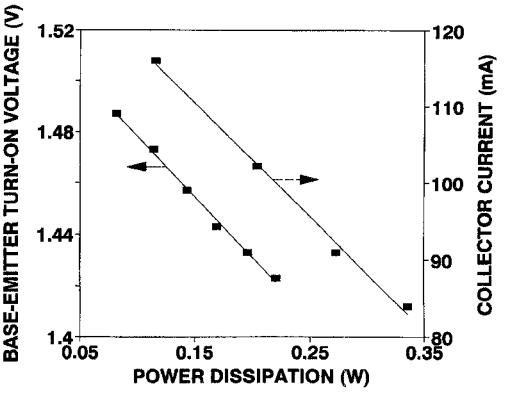

Fig. 3. Extraction of self-heating model parameters a and b from the measured power dependence of base-emitter turn-on voltage and collector current.

was 1 W while the maximum power-added efficiency was 56%.

The model extraction procedure is similar to that of [18] and [21]. First, linear parameters such as $R_{B2}, R_B, R_E, R_C, L_B, L_E$, and L_C and nonlinear parameters such as C_{BC} and C_{EX} were extracted from bias-dependent S-parameters, including those under an open-collector bias. Next, the forward diode characteristics were extracted from RF I-V waveforms while reverse diode characteristics were extracted from dc I-V characteristics. This procedure also yielded transit times such as τ_F, τ_R, and τ_C.

As described in Section II, the number of self-heating parameters were reduced to three, namely, a, b, and τ_{TH}. These parameters were extracted by comparing pulsed I-V characteristics under different pulse widths and duty factors as shown in Fig. 2. A plot of I_C as a function of pulse width under a fixed bias gives τ_{TH}. The slopes of dc I_C and V_{BE} versus power dissipation give a and b, respectively, as shown in Fig. 3.

For RF-breakdown characteristics, similar to [19], a 2 GHz signal was applied to either the base port with the HBT in forward operation, or to the collector port with the HBT in reverse operation. In both cases, the opposite port was terminated either in 50 Ω or a tuner. From the waveforms measured under these extreme bias conditions, the breakdown

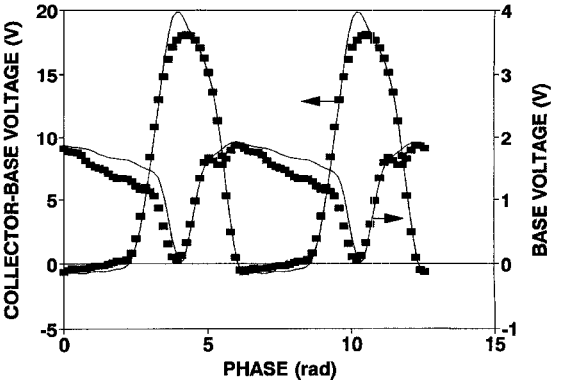

Fig. 4. (■) Measured versus (—) simulated base-emitter and collector-base voltage waveforms. V_{CE0} = 8 V. V_{BE0} = 1.3 V. P_{IN} = 21 dBm @ 2 GHz.

parameters were extracted. The resulted parameter values for the present HBT's are BV_{CEO} = 16 V; BV_{CBO} = 26 V; $\eta = 6.5$. These and other extracted parameter values are listed in Table I.

IV. SIMULATION AND DISCUSSION

The above extracted model has been implemented in a commercially available harmonic-balance circuit simulator,

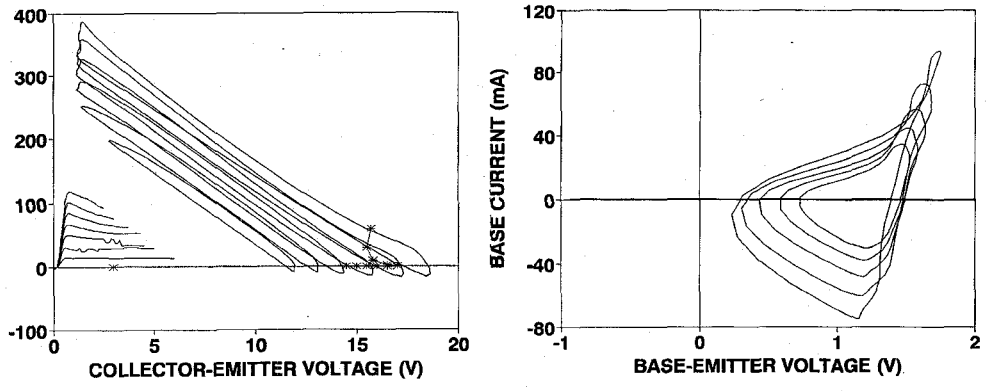

Fig. 5. Measured dynamic (a) load and (b) drive lines at the collector and base, respectively. The measured dc I-V and (*) breakdown characteristics are included in (a) for comparison. $V_{CE0} = 8$ V. $V_{BE0} = 1.3$ V. $P_{IN} = 11, 13 \cdots 21$ dBm @ 2 GHz.

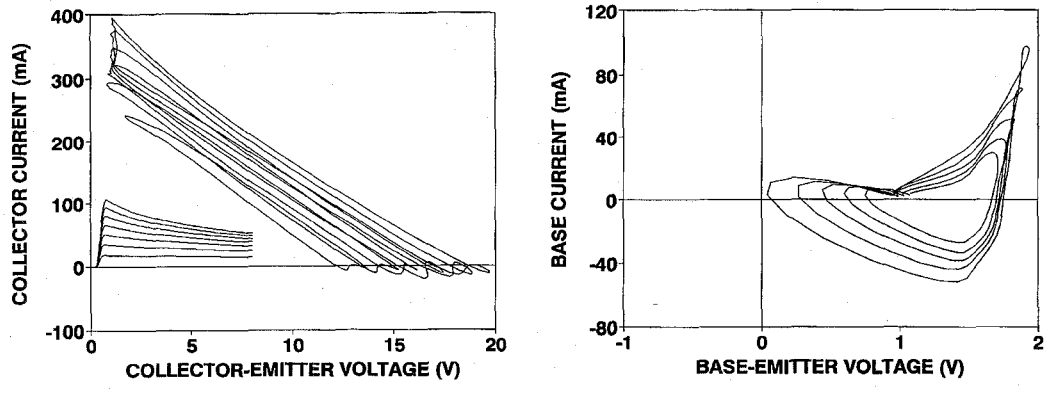

Fig. 6. Simulated dynamic (a) load and (b) drive lines at collector and base, respectively. The simulated dc I-V characteristics are included in (a) for comparison. $V_{CE0} = 8$ V. $V_{BE0} = 1.3$ V. $P_{IN} = 11, 13 \cdots 21$ dBm @ 2 GHz.

LIBRA [22], in terms of user-defined elements. This allows the breakdown effect on HBT power performance to be conveniently simulated and compared to the measured data. Since the simulation involves cases in which the HBT is severely overdriven, up to nine harmonics were used in the harmonic-balance simulation.

Initially, for both measurement and simulation, the HBT was operated in Class AB and driven with a 2 GHz signal. Fig. 4 shows that the measured and simulated base and collector voltage waveforms are in agreement. Fig. 5 shows the measured dynamic load and drive lines at the collector and base, respectively, when the drive level was stepped from 11 to 21 dBm so that the HBT was approximately 8 dB in compression. The measured dc collector characteristics are superimposed on Fig. 5(a). In comparison, the range covered by dc characteristics is rather limited in order to avoid strong thermal effects. Fig. 6 shows the simulated dynamic load and drive lines as well as dc characteristics. Again the simulated and measured characteristics are in good agreement.

Fig. 7 illustrates the agreement between the measured and simulated output power, power-added efficiency, and harmonic distortion. Both the measurement and simulation resulted in a maximum output power $P_{\rm OUT}^{\rm MAX}$ of 1.0 W which is much higher than what is allowed by conventional wisdom. Conventionally, $P_{\rm OUT}^{\rm MAX}$ for a common-emitter HBT can be estimated according to a simple formula:

$$P_{\rm OUT}^{\rm MAX} = I_{\rm MAX}(BV_{CEO} - V_{\rm SAT})/8. \tag{16}$$

Here the maximum collector current $I_{\rm MAX}$ is limited by either the self-heating or Kirk effect. For the present HBT's, both effects result in an $I_{\rm MAX}$ of approximately 400 mA. Since $BV_{CEO} = 16$ V and $V_{\rm SAT} = 1.6$ V, this implies a maximum output power of 0.7 W under a 40 Ω load. This apparent discrepancy is because the actual RF operation is far more complicated as discussed in the following.

According to the present model, $P_{\rm OUT}^{\rm MAX}$ is not necessarily limited by open-base breakdown. For example, under a Class B or C operation, the instantaneous collector voltage peaks when the base-emitter junction is reverse biased. Under a Class AB operation, even if the collector-base voltage peaks when the base-emitter junction is conducting, the collector-base voltage swings so rapidly that the junction capacitance presents a low impedance at the base. This allows the collector-emitter voltage to significantly exceed BV_{CEO}, hence higher $P_{\rm OUT}^{\rm MAX}$ than that predicted by (15). Fig. 4 confirms that the collector voltage peaks at 18 V. Fig. 8 compares the simulated power performance under common-emitter or common-base Class A, AB and C operations. In each case the load resistance R_L was chosen to maximize the output power while the input power was gradually increased until breakdown occurs. It can be seen

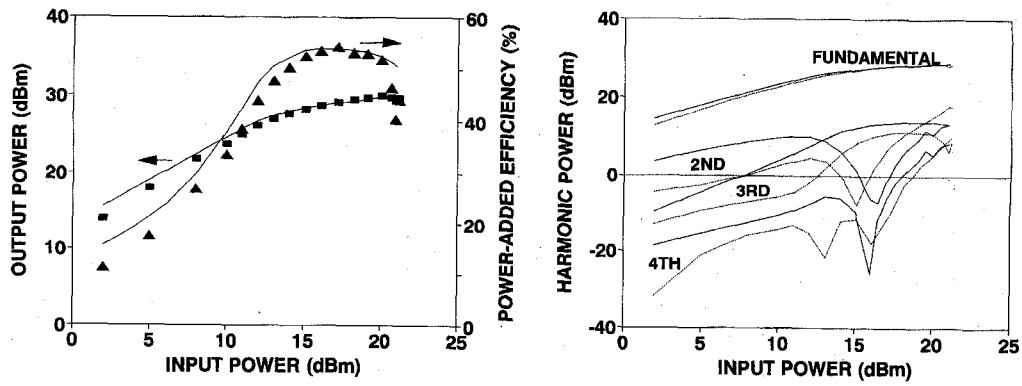

(a) (b)

Fig. 7. (symbol) Measured versus (curve) simulated (a) fundamental and (b) harmonic power performance at 2 GHz. $V_{CE0} = 8$ V. $V_{BE0} = 1.3$ V.

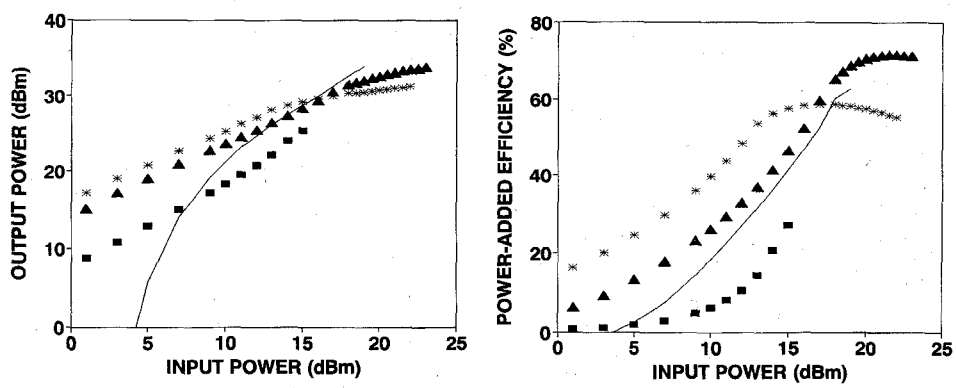

(a) (b)

Fig. 8. Simulated power performance under (■) common-emitter Class A: $V_{CE0} = 8$ V; $V_{BE0} = 1.65$ V; $R_L = 40$ Ω; common-emitter Class AB: $V_{CE0} = 8$ V; $V_{BE0} = 1.32$ V; $R_L = 40$ Ω; (—) common-emitter Class C: $V_{CE0} = 16$ V; $V_{BE0} = 0.5$ V; $R_L = 65$ Ω; (▲) common-base Class AB: $V_{CEO} = 12.5$ V; $V_{BE0} = 1.4$ V; $R_L = 68$ Ω.

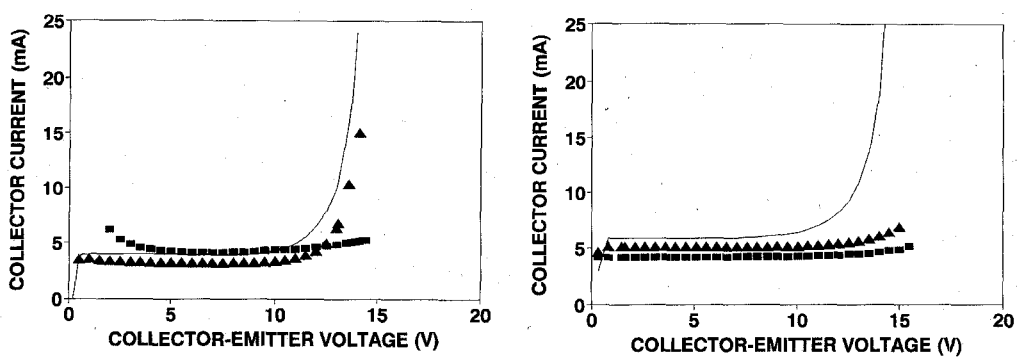

(a) (b)

Fig. 9. (a) Measured versus (b) simulated dc breakdown characteristics when the HBT is biased with a (■) constant voltage: $V_{BE} = 1.24$ V, (▲) shunt resistance: $V_{BE} = 1.24$ V, $R_{BL} = 50$ Ω, and (—) constant current: $I_B = 0.15$ mA.

that, except in the case of Class A operation, the output power continues to increase beyond 0.7 W. Such a power saturation behavior is different from that of a GaAs MESFET or PHEMT which can tolerate a certain amount of breakdown current so that additional power performance can be gained at the expense of long-term reliability [23]. In contrast, the HBT can tolerate little breakdown current and additional power performance is gained from actual improvement of breakdown voltage under different bias and drive conditions.

As shown in the appendix, the dc breakdown voltage is a function of the base external loading resistance R_{BL}:

$$BV_{CE} = BV_{CEO}\{[1 - \alpha_F/(1 + R_{BE0}/R_{BL})]/ \cdot (1 - \alpha_F)\}^{1/\eta}. \quad (17)$$

Thus, the breakdown voltage approaches BV_{CEO} when $R_{BL} = \propto$ but BV_{CBO} when $R_{BL} = 0$. Typically, R_{BL} is finite and the breakdown voltage is between BV_{CEO} and BV_{CBO}. Fig. 9 confirms that both the measured and

simulated breakdown voltages vary according to the base loading condition.

Under RF breakdown, the base load resistance is replaced with an impedance Z_{BL} which is a function of frequency. In particular, Z_{BL} can decrease with increasing frequency due to the shunting effect of junction or parasitic capacitances even without external base loading resistances. The decrease in Z_{BL} shifts the breakdown voltage from BV_{CEO} to BV_{CBO}, the latter being significantly higher than the former. Therefore, the maximum output power can significantly exceed the limit of open-base breakdown under favorable circuit design configurations. The examples include: 1) common-base configuration since BV_{CBO} is greater than BV_{CEO} in general; 2) Class B or C operation under which the collector voltage peaks when the base-emitter junction is reverse biased; 3) low base loading with constant voltage drive or a large shunt capacitance.

V. Conclusion

In summary, a large-signal HBT model including self-heating, collector transit-time, and RF-breakdown effects was developed. The model was verified through simulation and comparison with RF waveform and power measurements. The competing effect of open-base vs. open-emitter breakdown was analyzed. It is shown that open-base breakdown is not necessarily a limitation to the maximum power output and several circuit design configurations can be utilized to increase the output power. Such a large-signal model will be critical when the thermal resistance and nonuniformity of power HBT's are reduced so that electrical breakdown becomes the limiting factor for HBT performance and reliability.

Appendix

First consider dc breakdown while neglecting the parasitic recombination diode D_E. Under forward operation, the collector current can be expressed as in the following:

$$I_C = m_1\alpha_F I_E + m_2 I_{SC}. \tag{A1}$$

When the base is loaded with a shunt resistance R_{BL} the collector current equals

$$I_C = I_E - I_B + V_{BE}/R_{BL}. \tag{A2}$$

Let $R_{BE0} = V_{BE}/I_E$ and eliminate I_E between (A1) and (A2)

$$I_C = \{m_1\alpha_F I_B + m_2(1 + R_{BE0}/R_{BL})I_{SC}\}/ \cdot (1 - m_1\alpha_F + R_{BE0}/R_{BL}). \tag{A3}$$

Thus, I_C approaches infinity when

$$m_1\alpha_F = 1 + R_{BE0}/R_{BL}. \tag{A4}$$

Eliminate m_1 between (A4) and (11), we have the corresponding breakdown voltage

$$BV_{CB} = BV_{CEO}\{[1 - \alpha_F/(1 + R_{BE0}/R_{BL})]/ \cdot (1 - \alpha_F)\}^{1/\eta}. \tag{A5}$$

References

[1] P. C. Grossman and J. Choma, "Large signal modeling of HBT's including self-heating and transit-time effects," *IEEE Trans. Microwave Theory Tech.*, vol. 40, pp. 449–464, Mar. 1992.

[2] P. Baureis, D. Seitzer and U. Schaper, "Modeling of self-heating in GaAs/AlGaAs HBT's for accurate circuit and device analysis," in *Tech. Dig. IEEE GaAs IC Symp.*, Oct. 1991, pp. 125–128.

[3] C. McAndrew, "A complete and consistent electrical/thermal HBT model," in *IEEE Bipolar Circuits Technol. Meet. Proc.*, 1992, pp. 10.1.1–10.1.4.

[4] Q. M. Zhang, J. Hu, J. Sitch, R. K. Surridge, and J. M. Xu, "A new large-signal HBT model," in *IEEE MTT-S Int. Microwave Symp. Dig.*, May 1994, pp. 1253–1256.

[5] V. Krozer, M. Ruppert, W. Y. Lee, J. Grajal, A. Goldhorn, M. Schussler, K. Fricke, and H. L. Hartnagel, "A physics-based temperature-dependent SPICE model for the simulation of high- temperature microwave performance of HBT's and experimental results," in *IEEE MTT-S Int. Microwave Symp. Dig.*, May 1994, pp. 1261–1264.

[6] K. Lu, P. Perry, and T. J. Brazil, "A new SPICE-type heterojunction bipolar transistor model for dc, microwave small-signal and large-signal circuit simulation," in *IEEE MTT-S Int. Microwave Symp. Dig.*, May 1994, pp. 1579–1582.

[7] A. Samelis and D. Pavildis, "Heterojunction bipolar transistor large-signal model for high-power microwave application," in *IEEE MTT-S Int. Microwave Symp. Dig.*, May 1995, pp. 1231–1234.

[8] R. Hajji, A. B. Kouki, S. E. Rabaie, and F. M. Ghannouchi, "Systematic dc/small-signal/large-signal analysis of heterojunction bipolar transistors using a new consistent nonlinear model," *IEEE Trans. Microwave Theory Tech.* vol. 44, pp. 233–240, Feb. 1996.

[9] D. A. Teeter, J. R. East, R. K. Mains, and G. I. Haddad, "Large-signal numerical and analytical HBT models," *IEEE Trans. Microwave Theory Tech.*, pp. 837–844, May 1993

[10] P. Baureis and D. Seitzer, "Parameter extraction for HBT's temperature dependent large signal equivalent circuit model," in *Technical Dig. IEEE GaAs IC Symp.*, Oct. 1993, pp. 263–266.

[11] K. Lu, P. A. Perry and T. J. Brazil, "A new large-signal AlGaAs/GaAs HBT model including self-heating effects, with corresponding parameter-extraction procedure," *IEEE Trans. Microwave Theory Tech.*, vol. 43, pp. 1433–1445, July 1995.

[12] N. Wang, N. Sheng, M. Chang, W. Ho, G. Sullivan, E. Sovero, J. Higgins, and P. Asbeck, "Ultrahigh power efficiency operation of common-emitter and common-base HBT's at 10 GHz," *IEEE Trans. Microwave Theory Tech.*, vol. 38, pp. 1381–1389, Oct. 1990.

[13] M. G. Adlerstein and M. D. Zatlin, "Cutoff operation of heterojunction bipolar transistors," *Microwave J.*, pp. 114–125, Sept. 1991.

[14] D. S. Whitefield, C. J. Wei, and J. C. M. Hwang, "Temperature-dependent large-signal model of heterojunction bipolar transistors," in *Tech. Dig. IEEE GaAs IC Symp.*, Oct. 1992, pp. 221–224.

[15] ——, "Elevated temperature microwave characteristics of heterojunction bipolar transistors," in *Tech. Dig. IEEE GaAs IC Symp.*, Oct. 1993, pp. 267–270.

[16] B. R. A. Sugeng, C. J. Wei, J. C. M. Hwang, W. P. Hong, J. I. Song, and J. Hayes, "A physically based SPICE model for microwave double heterojunction bipolar transistor," in *Dig. IEEE Sarnoff Symp.*, Mar. 1993.

[17] B. R. A. Sugeng, C. J. Wei, J. C. M. Hwang, J. I. Song, W. P. Hong, and J. R. Hayes, "Junction barrier effects on the microwave power performance of double heterojunction bipolar transistors," in *Proc. IEEE/Cornell Conf. Advanced Concepts in High Speed Semiconductor Devices and Circuits*, Aug. 1993, pp. 52–61.

[18] C. J. Wei, Y. E. Lan, J. C. M. Hwang, W. J. Ho, and J. A. Higgins, "Waveform-based modeling and characterization of microwave power heterojunction bipolar transistors," *IEEE Trans. Microwave Theory Tech.*, vol. 43, pp. 2899–2903, Dec. 1995.

[19] C. J. Wei, J. C. M. Hwang, W. J. Ho, and J. A. Higgins, "Large-signal modeling of self-heating and RF-breakdown effects in power HBT's," in *Dig. IEEE MTT-S Int. Microwave Symp.*, June 1996, pp. 1751–1754.

[20] H. C. Chung, M. D. Wetzel, and J. C. M. Hwang, "Instantaneous burn-out, long-term burn-out and gradual degradation of HBT's," in *Programs Abstract GaAs Reliability Workshop*, pp. 11–13, Oct. 1995.

[21] C. J. Wei and J. C. M. Hwang, "New method for direct extraction of HBT equivalent circuit parameters," *IEEE Trans Microwave Theory Tech.*, vol. 43, pp. 2035–2040, Sept. 1996.

[22] HP-EEsof, Westlake Village, CA 91362 USA.

[23] J. C. M. Hwang, "Gradual degradation under RF overdrive of MESFET's and PHEMT's," in *Tech. Dig. IEEE GaAs IC Symp.*, Oct. 1995, pp. 81–84.

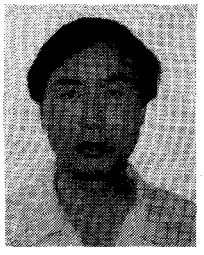

Ce-Jun Wei (M'93) received the B.S. degree from Qinghua University, China, in 1962 and the Ph.D. degree from Chinese Academy of Sciences in 1966, both in electrical engineering.

From 1966 to 1989, he worked on the modeling and characterization of microwave devices and circuits at the Semiconductor Institute of Chinese Academy of Sciences. Between 1980 and 1982, he was also a Visiting Professor at the Technical Institute of Aachen, Germany. Between 1986 and 1988, he was a Visiting Professor at Heinrich-Hertz-Institute and Berlin Technical University. In 1989, he joined Lehigh University where he is currently Senior Research Scientist of Compound Semiconductor Technology Laboratory. His research interest covers modeling and characterization of microwave devices and circuits, as well as optoelectronics. He has published more than 40 technical papers.

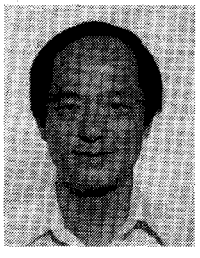

James C. M. Hwang (M'81–SM'82–F'94) graduated from National Taiwan University with a B.S. degree in Physics in 1970. He received his M. S. and Ph. D. in Materials Science and Engineering from Cornell University in 1973 and 1976, respectively.

He had 12 years of industrial experience working at IBM, AT&T, GE, and Gain Electronics. In 1988, he joined Lehigh University, Bethlehem, PA, as Professor of Electrical Engineering and Director of Compound Semiconductor Technology Laboratory. He has been a consultant for the Air Force Wright Laboratory and several private companies. He is a co-founder and director of Quantum Epitaxial Designs, Inc. His interest in compound semiconductors ranges from material and processing to devices and circuits. He has published over 100 papers and been granted four patents in these areas.

Wu-Jing Ho (M'88) graduated with the B.S. degree in 1973 and the M.S. degree in 1975 from National Tsing Hua University, Taiwan, both in chemistry. He received the Ph.D. degree in materials science from University of Southern California in 1981.

He then worked on advanced silicon devices and GaAs MESFET's until joining Rockwell Science Center in 1986. Since then, he has been active in GaAs- and InP-based HEMT's and HBT's for digital and microwave/millimeter-wave circuits. He participated in transferring the tungsten-silicide-gate MESFET process from IBM to Rockwell. His accomplishments include BiFET LSI technology, multifunctional HBT technology, high-power/high-efficiency HBT MMIC's, high-yield HEMT SRAM's, and HEMT/Schottky-diode IC's. He has over 40 technical publications, one patent, and three patents pending.

J. Aiden Higgins (M'62–SM'78) graduated with the B.E. (Hons.) from Dublin University in 1958. He received the M.S. degree in 1964 and the Ph.D. in 1971 from Stanford University, both in electrical engineering.

He joined Rockwell, Thousand Oaks, CA, in 1971 where he is currently Manager of the Millimeter-Wave Devices Department at the Science Center. At Rockwell, he led the development of IR detectors and GaAs MESFET's. He pioneered the use of direct ion-implantation and doping-profile tailoring in MESFET fabrication. He was among the first to demonstrate microwave monolithic IC's with active on-chip matching. He designed GaAs CCD's with an agile bandpass filter and a spatial light modulator. He has exploited the use of HEMT's and HBT's for millimeter-wave applications, resulting in state-of-the-art low-noise InGaAs HEMT's and high-power AlGaAs/GaAs HBT's. Currently, his research activities include innovative millimeter-wave power combining and packaging. He has over 50 publications and three patens in the area of GaAs devices.